Supplement of:

Assessment of Remote Sensing Reflectance Glint Correction Methods from Fixed Automated Above-Water Hyperspectral Radiometric Measurement in Highly Turbid Coastal Waters

BEHNAZ ARABI, MASOUD MORADI, ANNELIES HOMMERSOM, JOHAN VAN DER MOLEN AND LEON SERRE-FREDJ

S1- Estimation of $b_{bp}(\lambda)$ from $b_p(\lambda)$

In this study, we used the measured $b_p(\lambda)$ and $b_{bp}(\lambda)$ dataset by Röttgers et al. (2023) in the Wadden Sea (https://doi.pangaea.de/10.1594/PANGAEA.954981). The Total Suspended Sediment (TSS) and Turbidity showed strong correlation with $b_p(\lambda)$ in oceanic (North Sea), coastal and estuaries regions of the Wadden Sea (Fig. S1). About 94% of sample data lied in the 95% confidence limit of variations. This indicates that the material scattering varied in a systematic way with increasing turbidity. Therefore, a trend of $b_p(\lambda)$ from oceanic, coastal, and estuary indicated the scattering phase and variability of the particle backscattering ratio.

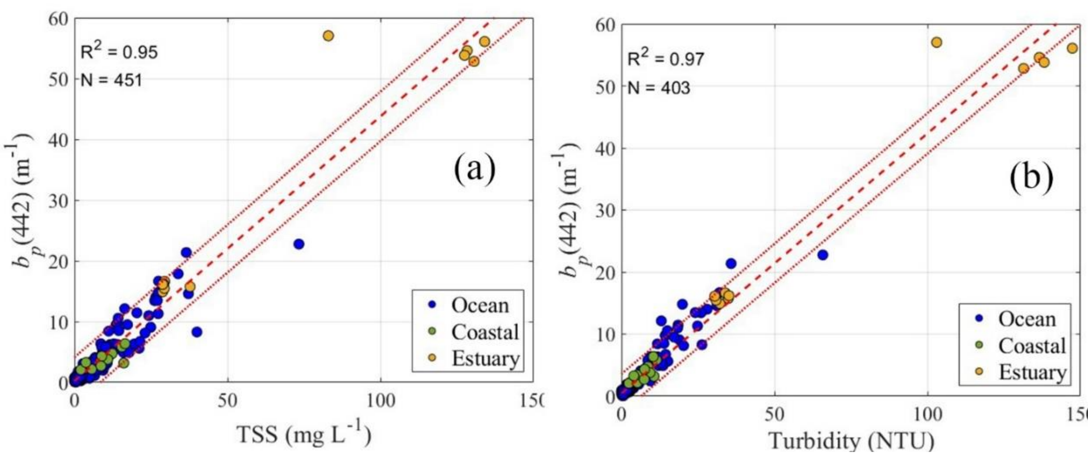

Fig. S1- Correlation between TSS (a) and Turbidity and $b_p(442)$ using in-situ data. The dashed and dotted lines show the linear fits and the upper and lower bounds of 95% confidence level, respectively.

The $b_{bp}(\lambda)$ of water components are determined by:

$$b_{bp}(\lambda) = b_p(\lambda) \times B \tag{S1}$$

where B is the backscattering ratio. Two approaches were considered to analyze the variability of $\boldsymbol{B}$ values (McKee et al., 2009), include: (i) point-by-point where $\boldsymbol{B}$ was calculated by dividing

$b_{bp}(\lambda)$ by the corresponding individual $b_p(\lambda)$ measurements. The variability of ***B*** was analyzed using statistical metrics of the particle backscattering ratio distribution. (ii) regression analysis where the best fit values of $b_{bp}(\lambda)/b_p(\lambda)$ for the whole measured dataset was calculated. To minimize the measurement uncertainties for both $b_{bp}(\lambda)$ and $b_p(\lambda)$, the geometric mean regression model, known as the "Least Suares Bisector" (LSB) for Model II regression algorithm was used to analyze the spectral variability of ***B*** values (**https://www.mbari.org/technology/matlab-scripts/linear-regressions/**). Since the bands at $\lambda \leq 440$ nm and $\lambda \geq 700$ nm introduced significant uncertainties in the spectral variability analysis, they were excluded from our analysis (Zhang et al., 2010)**.**
Fig. S2 shows the correlation between measured $b_{bp}(\lambda)$ and $b_p(\lambda)$ at different wavelengths. About 92% of dataset lied in the 95% confidence level of $b_{bp}(\lambda)$ and $b_p(\lambda)$ variations. The outlier data may be due to variations in the material composition that change with increasing turbidity, and possibly also due to the performance limitations of field measurements. A linear relationship was found in Fig. S2 for all wavelengths. Hereafter, the results were presented for dataset which lie in the 95% confidence level of $b_{bp}(\lambda)$ vs. $b_p(\lambda)$. The value of $b_{bp}(\lambda)/b_p(\lambda)$ values in Fig.S3 were 0.0330, 0.0277, 0.0260, and 0.0268 with 95% confidence intervals of ± 0.0002 for bands 442, 488, 510, and 620, respectively. The maximum relative error of 30.4% was observed between bands 420nm and 510nm. The offsets in Fig. S2 were unexpected, as the zero values of $b_p(\lambda)$ and $b_{bp}(\lambda)$ should have coincided (Eq. S1). This could be due to an underestimation of b_{bp}, an overestimation of b_p, or a combination of both. Fig. S3 shows the correlations of TSS with $b_p(\lambda)$ and $b_{bp}(\lambda)$. The positive offset of the linear fits in the correlation between TSS and $\boldsymbol{b_p}(\lambda)$ revealed underestimation of TSS or overestimation of b_p (Δb_p). Meanwhile, the positive offset between TSS and $b_{bp}(\lambda)$ showed underestimation of TSS or overestimation of b_{bp} (Δb_{bp}). Therefore, the non-zero offset in Fig. S2 resulted possibly from overestimation of b_p and b_{bp}.
The values of Δb_p and Δb_{bp} were calculated using the geometric mean regression LSB-Model II from dataset of Fig. S3a-d and Fig. 3f-h, respectively. The values of Δb_p were 0.1592, 0.1585, 0.1579, and 0.1617 for bands 442, 488, 510, and 620 nm, respectively. The values of Δb_{bp} were 0.0016, 0.0009, 0.0021, and 0.0022 for bands 442, 488, 510, and 620 nm, respectively. Fig. 4S shows the mean values of backscattering ratio, *B*, at different wavelengths after correction of Δb_p and Δb_{bp}. The mean values of point-by-point *B* were 0.0256±0.0027 at wavelengths 442-620 nm (Fig. S4a). Fig. S4b shows the LBS-Model II regression of backscattering ratio at different wavelengths and associated 95% confidence intervals of ***B***. The LSB-Model II regression determined a narrow confidence intervals of backscattering ratio, with a mean value of 0.0261±0.0002. As a result, the backscattering ratio could be regarded as wavelength-independent due to the measurements associated with $b_p(\lambda)$ and $b_{bp}(\lambda)$ in the range of 442-620 nm.

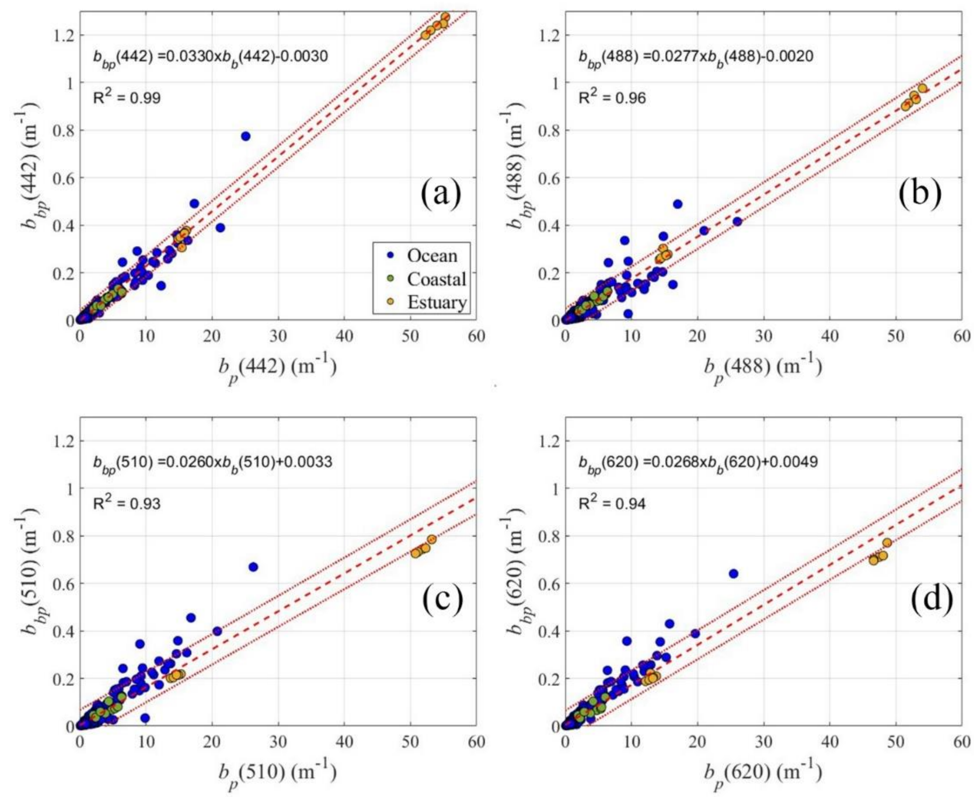

Fig. S2- Correlation between b_p and b_{bp} at 442 nm (a), 488 nm (b), 510 nm (c), and 620 nm (d). The dashed and dotted lines show the linear fits and the upper and lower bounds of 95% confidence level, respectively. N = 483.

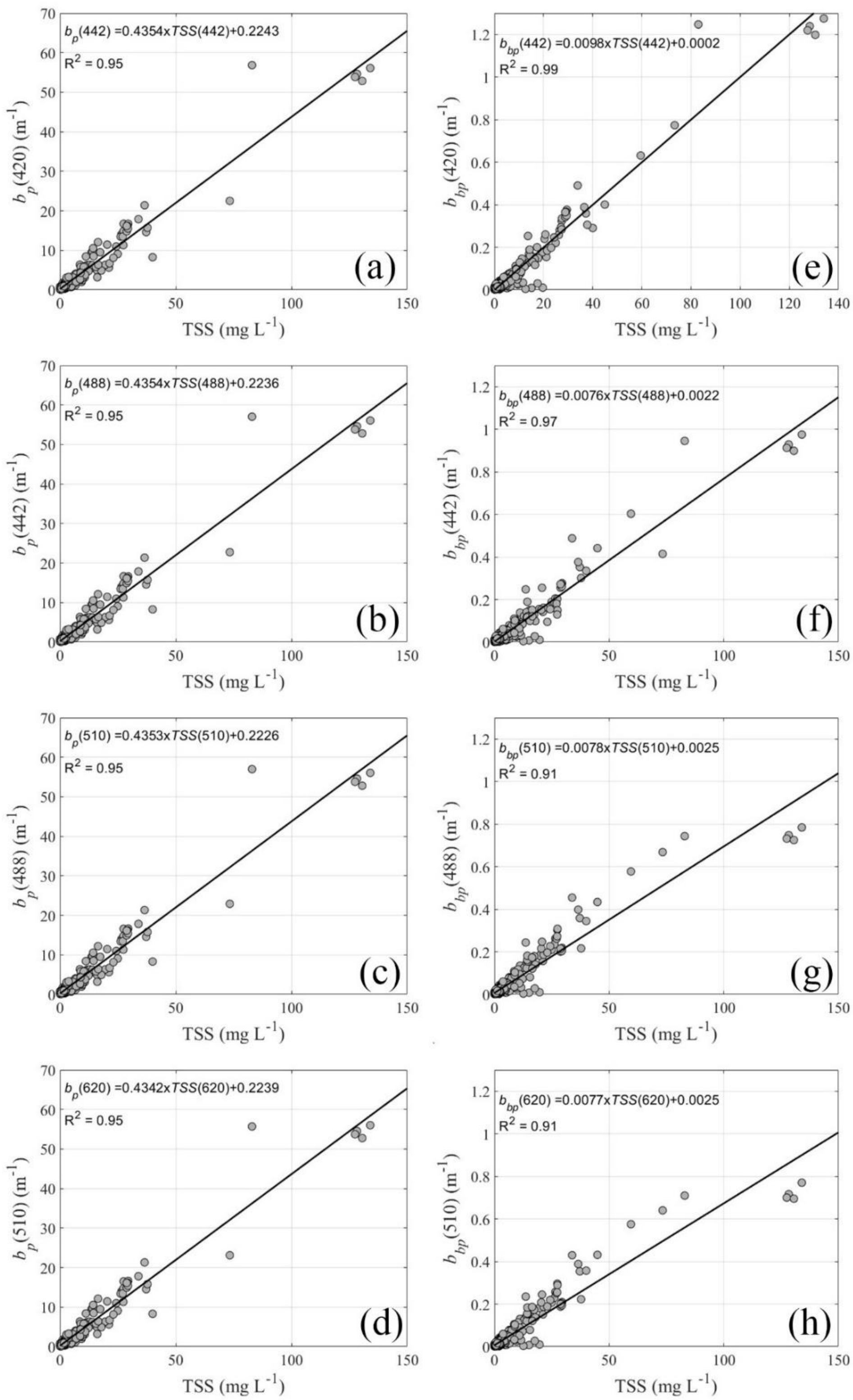

Fig. S3- Correlation between TSS and b_p (left column) and b_{bp} (right column). The solid lines show the best linear fits. N = 451.

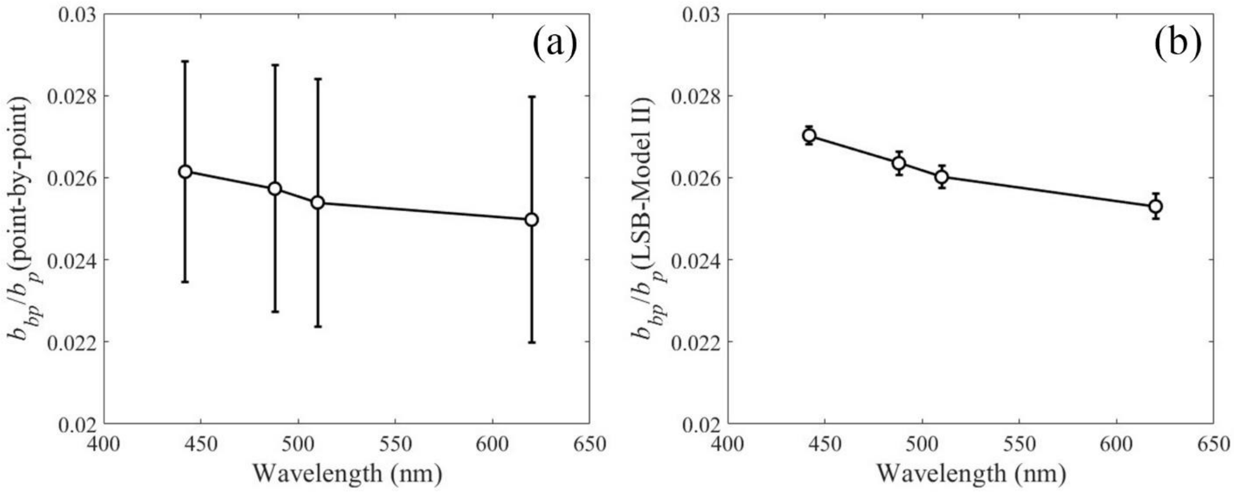

Fig. S4- a) variation of backscattering ratio at different wavelength using the point-by-point method. Error bars show ±1 standard deviation**. b)** similar to (a), but calculated using the LSB-Model II regression method. Error bars show tight confidence intervals.

S2- Statistical Parameters

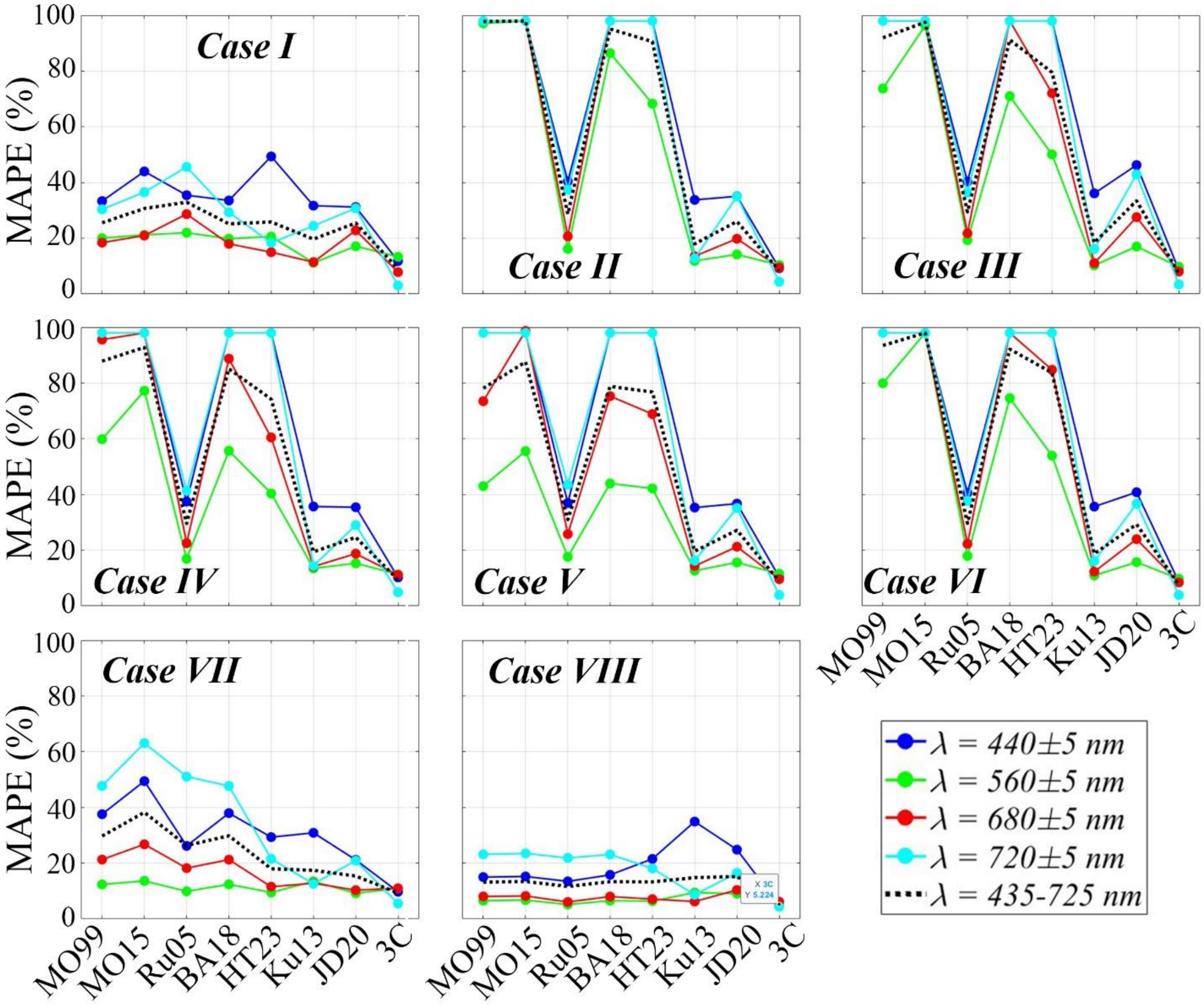

Fig. S5. The MAPE between $R_{rs,ref}(\lambda)$ and modeled $R_{rs}(\lambda)$ in different environmental conditions (*Case I* - *Case VIII*). The environmental conditions are illustrated in the text.

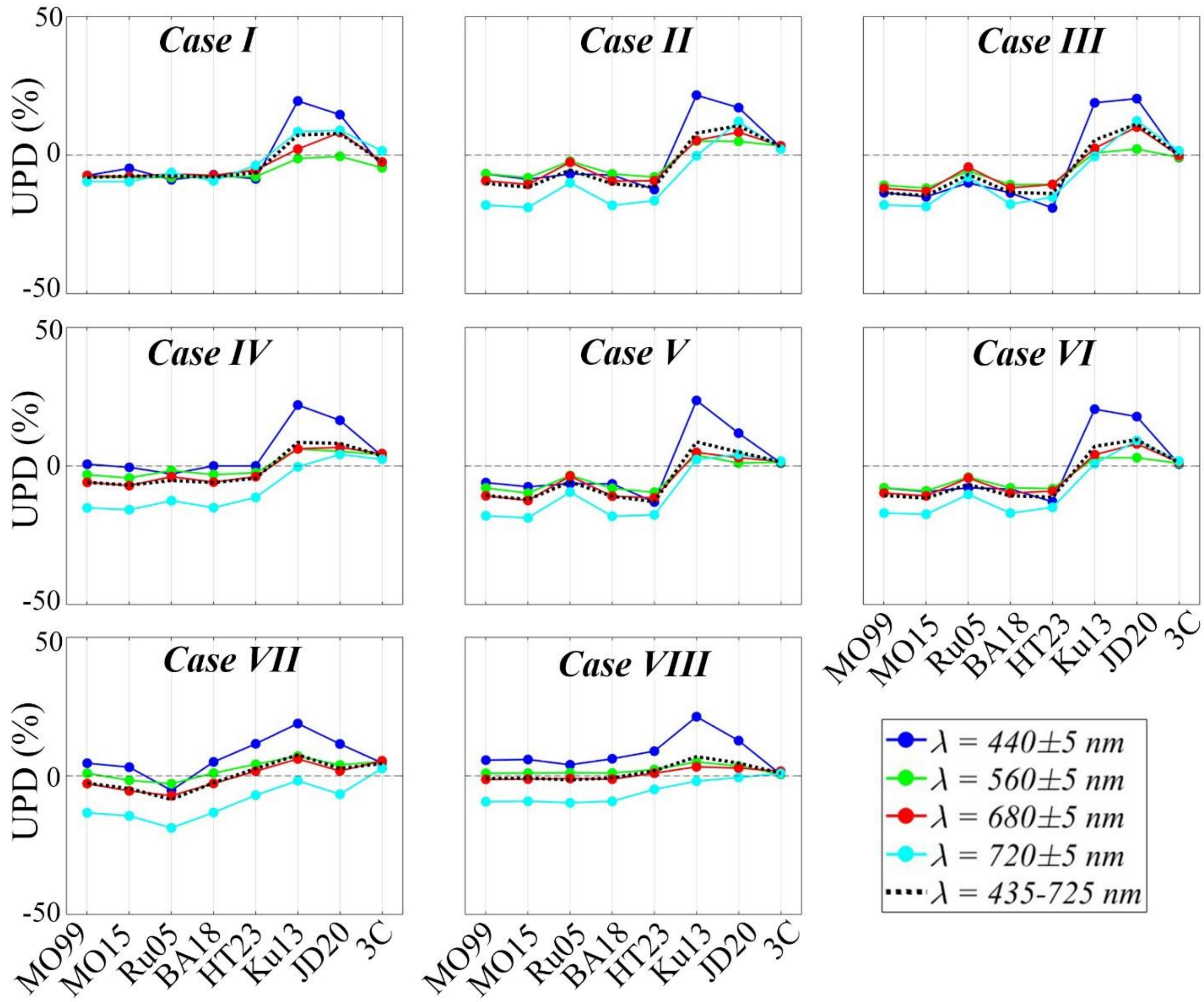

Fig. S6. The UPD values between $R_{rs,ref}(\lambda)$ and modeled $R_{rs}(\lambda)$ in different environmental conditions (*Case I* - *Case VIII*). The environmental conditions are illustrated in the text.

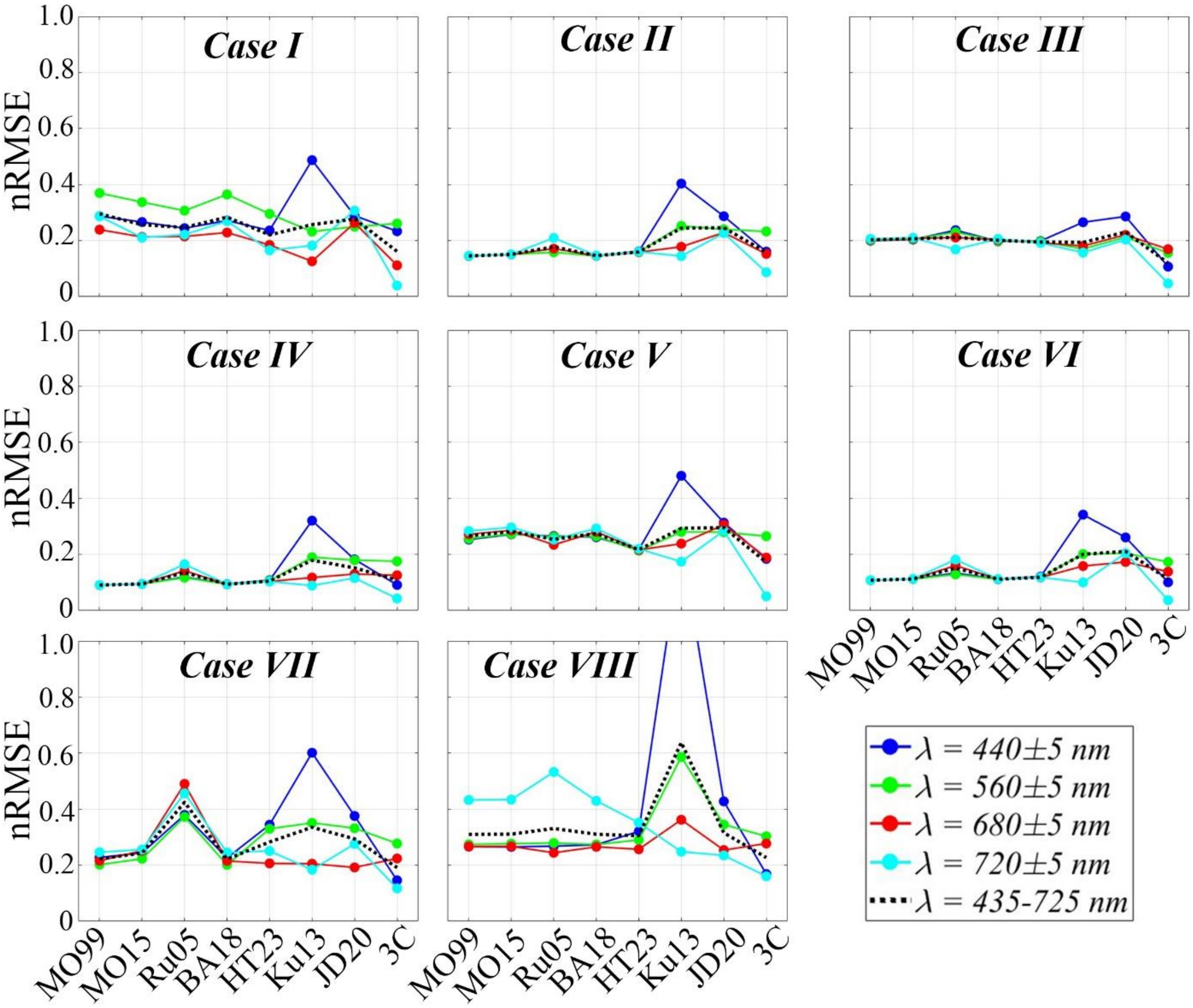

Fig. S7. The nRMSE values between $R_{rs,ref}(\lambda)$ and modeled $R_{rs}(\lambda)$ in different environmental conditions (*Case I* - *Case VIII*). The environmental conditions are illustrated in the text.

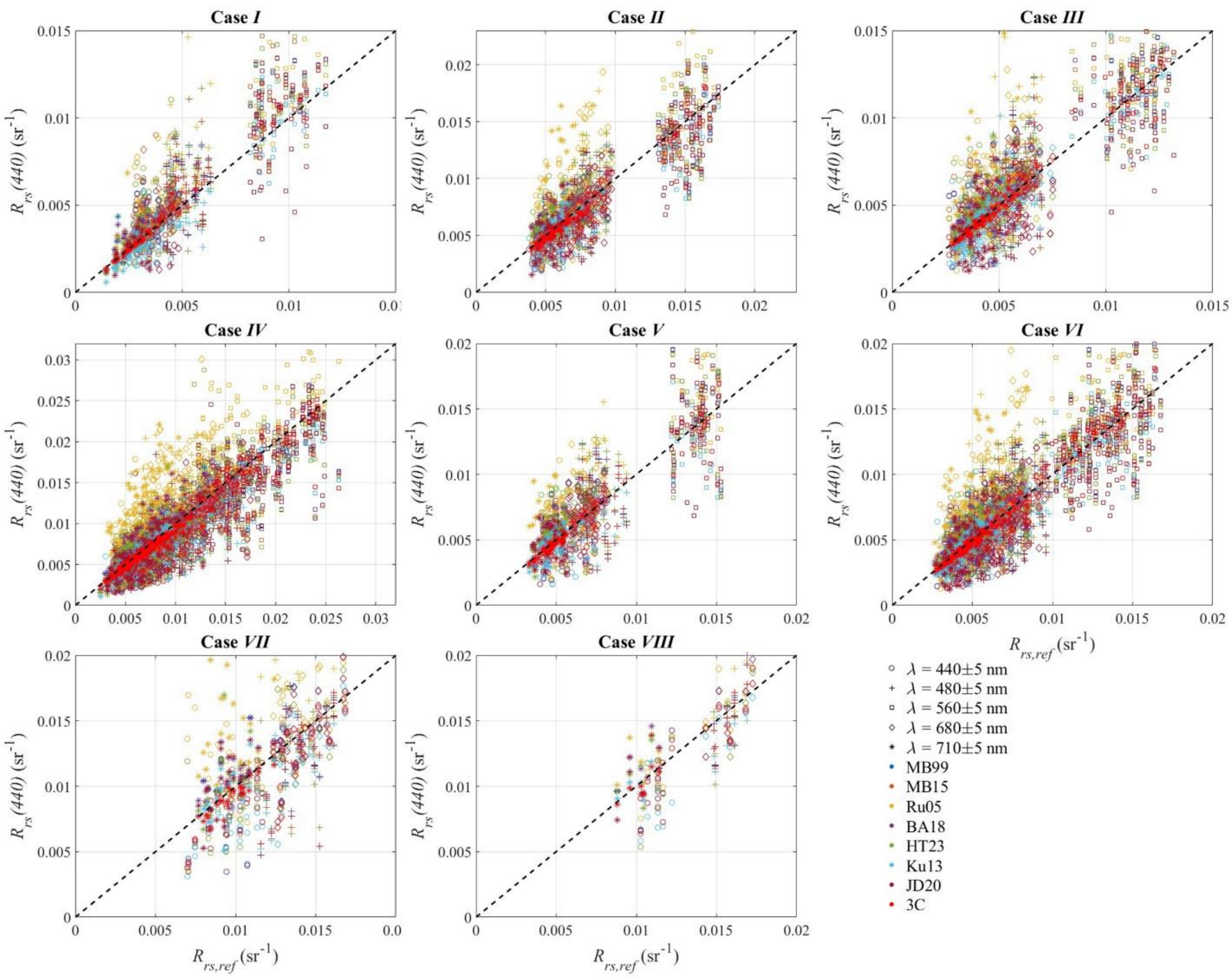

Fig. S8. Scatterplots of $R_{rs,ref}(\lambda)$ vs. estimated $R_{rs}(\lambda)$ using different models at selected blue, green, red, and NIR wavelengths in different environmental conditions (*Case I* - *Case VIII*). The environmental conditions are illustrated in the text.

Reference:

Röttgers, R., Bi, S., Burmester, H., Heymann, K., Hieronymi, M., Krasemann, H., Schönfeld, W., 2023. Water inherent optical properties and concentrations of water constituents from the German Bight and adjacent regions. https://doi.org/10.1594/PANGAEA.950774